Comprehensive Study on the Loss of Protectiveness Behavior in Cr-Coated ATF in High-Temperature Steam Oxidation

Dongju Kim, Youho Lee *
Seoul National University, 1 Gwanak-ro, Gwanak-gu, Seoul 08826, Korea
**Corresponding author: leeyouho@snu.ac.kr*

***Keywords: Accident Tolerant Fuel, Cr coating, Diffusion, Oxidation, Protectiveness**

1. Introduction

Cr-coated accident tolerant fuel cladding effectively reduces the oxidation of the fuel cladding during the steady state operation or high temperature accidental conditions by applying Cr-coating on the outer surface of the cladding. The oxidation resistance was confirmed throughout numerous studies [1, 2] and it can be maintained under moderate accident conditions within the envelope of design basis accident (DBA). On the other hand, Cr-coated cladding exhibits complex diffusion and oxidation behaviors under high temperature, and it can lose its protectiveness for exposure to long-term oxidation [1, 3].

The most important mechanism for loss of protection and oxidation of Cr-coated cladding is the diffusion of zirconium through the chromium's grain boundaries, followed by oxygen transfer after the zirconium has penetrated the entire coating. This phenomenon is based on the following mechanisms:

① Diffusion and oxidation loss of Cr-coating
② Recrystallization of Cr-coating
③ Diffusion of Zr through recrystallized grain boundaries of Cr-coating
④ Reduction of Cr_2O_3 and inner Zr oxidation

The schematic diagram of the framework to model the loss of protection and oxidation based on those mechanisms is given in **Fig. 1**. It is essential to determine both the required length for zirconium diffusion and the number density of these diffusion sites. The necessary diffusion length corresponds to the instantaneous thickness of the coating as it undergoes oxidation, which can be modeled by considering both the oxidation and diffusion losses of the coating. The number of zirconium path is equal to the grain boundary density of coating, and it can be modeled by recrystallization of coating. By combining these two models, the required diffusion length and site density of zirconium diffusion could be determined, which subsequently gives a boundary condition for chromium oxide reduction and oxygen ingress models. Since each model is significantly influenced by coating fabrication, it is necessary to develop models through experiments that take into account the coating effects.

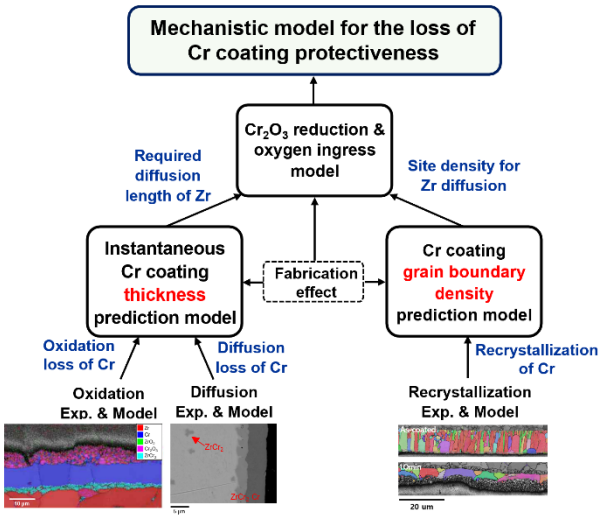

Fig. 1. Schematic diagram for modeling framework of the loss of protection and oxidation of Cr-coating

In this study, experiments and comprehensive investigations were conducted, and preliminary result for develop each separate model to predict the loss of protection and oxidation behavior of Cr-coated cladding was presented. Three different types of Cr-coated cladding tubes were exposed to prolonged high temperature steam oxidation using thermogravimetric analysis (TGA), and the loss of protection behaviors were observed. After the experiment, various equipment such as Transmission Electron Microscopy (TEM), Scanning Electron Microscopy (SEM), Transmission Kikuchi Diffraction (TKD), and Electron Backscatter Diffraction (EBSD) were used to capture the microstructure changes during the loss of protection.

2. Methodology

Three different types of coating were used in experiments (**Table. 1**). One specimen was coated using the magnetron sputtering method, and two specimens were coated using the arc ion plating method with different coating thicknesses. Each specimen was sealed at both ends with ceramic plugs to eliminate inner side oxidation. The specimen was oxidized at 1100 to 1300 ℃ using TGA with in-situ weight gain measurement. Each specimen was heated at a rate of 50 K/min up to the target temperature and then maintained at the temperature for various durations. After the experiment, the

microstructural changes were investigated using various equipment such as SEM, EBSD, TEM, TKD, and EPMA.

Table. 1. Base material and coating parameters

Base material	Coating method	Coating thickness
Zr-1.1Nb alloy	Magnetron sputtering	13.5 μm
	Arc ion plating	16 μm
		12 μm

3. Results & Discussion

3.1 Oxidation behavior of Cr-coated cladding

The measured weight gain of Cr-coated (12 μm) cladding at 1200 ℃ was compared with the weight gain of uncoated cladding (**Fig. 2**). While the uncoated cladding shows a decreasing rate of oxidation over time, a parabolic growth, the Cr-coated cladding shows very slow oxidation in early phase. But at a certain point, a transition occurs, and the oxidation rate increases rapidly. Within the time corresponding to an ECR of less than 17%, which is the allowable limit for DBA, the oxidation rate of Cr-coated cladding is up to 50 to 5 times slower than uncoated one. However, under extended oxidation conditions, a transition occurs, and it can increase up to twice than the rate of uncoated cladding.

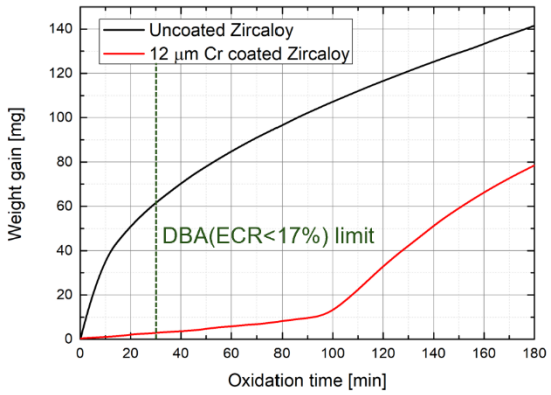

Fig. 2. Measured weight gain of uncoated & Cr-coated (12 μm) Zircaloy during the steam oxidation at 1200 ℃.

3.2 Oxidation and Diffusion loss of Cr-coating

The post-oxidation microstructure of Cr-coated specimen is depicted in **Fig. 3**. As shown in the figure, chromium oxide (Cr_2O_3) layer forms at the outer surface, and $ZrCr_2$ intermetallic layer forms at the zirconium-chromium interface and the thicknesses of both layers increasing over time. The thickness of residual Cr-coating layer decreases over time, by the combined effects of oxidation loss due to the formation of Cr_2O_3 layer and diffusion loss from the formation of the $ZrCr_2$ layer.

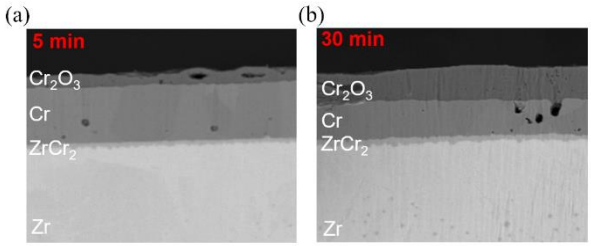

Fig. 3. Cross-sectional SEM image of Cr-coated (16 μm) Zircaloy during the oxidation at 1200 ℃: (a) 5 minutes. (b) 30 minutes.

Combining the oxidation loss model [4] and diffusion loss model [5], the remaining Cr-coating layer thicknesses were predicted and compared with measured thicknesses (**Fig. 4**). For the tested temperature range, residual Cr-coating layer thicknesses can be predicted within an error margin of about 10% for most cases by combining the two models. This result implying that the transient Cr-coating thickness can be modeled by employing diffusion loss and oxidation loss model. In the case of specimen exposed to extended time, the measured thicknesses were slightly larger than predicted. The microstructure of this specimen presented in **Fig. 4** shows that difference may be due to the partial reduction of the Cr_2O_3 layer, which may slow down the oxidation loss of Cr-coating.

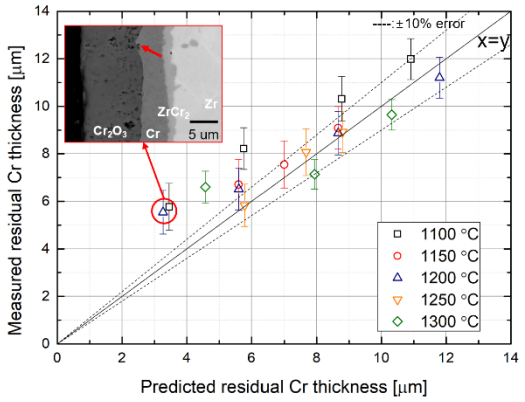

Fig. 4. Comparison of predicted and measured residual Cr-coating layer thickness.

3.3 Recrystallization of Cr-coating

The Cr-coating has columnar grain structure with a width of about 1 micrometer before oxidation, and these grains rapidly recrystallize when exposed to high temperatures. The recrystallization for three different specimen and three different oxidation temperature (1100, 1200, and 1300 ℃) were investigated. The result for 13.5 μm was given for example in this paper. **Fig. 5** is the EBSD map shows the recrystallization behavior of the Cr-coating layer oxidized at 1100 ℃. It shows that small grains of as-coated specimen grow over time, and it forms grains with width of 10~20 μm.

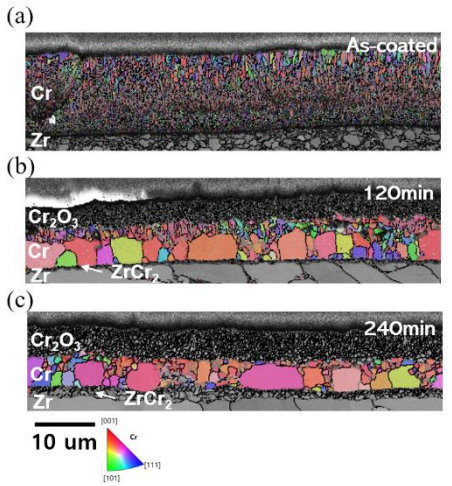

Fig. 5. EBSD IPF map of Cr-coated (13.5 μm) Zircaloy during the oxidation at 1100 ℃: (a) as-received. (b) 120 minutes. (b) 240 minutes.

The average grain boundary density was obtained using image analysis for the EBSD map data (**Fig. 6**). The grain boundary density is crucial as it determines the density of the diffused Zr, which acts as an oxygen path. Hence, it is closely related to the oxidation behavior of the Cr-coated cladding after loss of protection. As can be seen in the figure, the grain boundary density gradually decreases over time and the saturated values were similar between the oxidation temperatures.

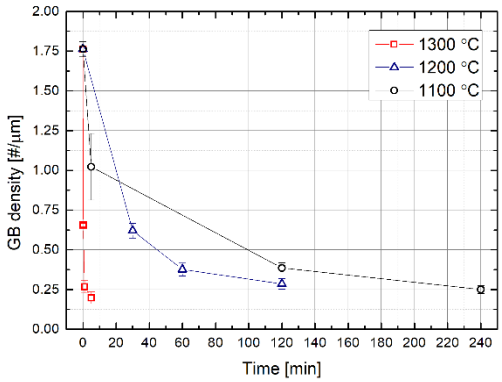

Fig. 6. Grain boundary density change of Cr-coated (13.5 μm) Zircaloy during the oxidation at 1100-1300 ℃.

3.4 Diffusion of Zr through recrystallized grain boundaries of Cr-coating

Due to the very low solubility and slow diffusion of zirconium in chromium, zirconium diffuses along the grain boundaries of chromium instead of bulk diffusion. **Fig. 7** shows the EBSD-EDS analysis of a 16 μm Cr-coated specimen that lost its protection after being oxidized at 1200 ℃ for 2.5 hours. It is shown that the locations of zirconium diffusion, as seen in the EDS analysis (**Fig. 7(b)**), were identical to the location of grain boundaries identified in the IPF map (**Fig. 7(c)**). Additionally, the depth of zirconium diffusion was found to be about 5~6 μm, identical to the thickness of the remaining chrome layer, which indicates that the diffused zirconium penetrating the entire coating.

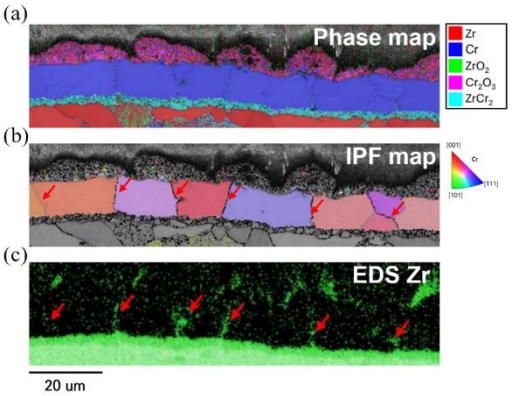

Fig. 7. EBSD-EDS analysis of Cr-coated (16 μm) Zircaloy specimen oxidized at 1200 ℃ for 2.5 hours: (a) Phase map. (b) IPF map. (c) EDS mapping (Zr).

The TKD-TEM analysis was conducted to capture the phase and microstructure of diffused zirconium. The TKD results (**Fig. 8(a)**) shows the diffused zirconium exists as a ZrO_2 phase along the chromium coating grain boundaries, and it is in contact with the $ZrCr_2$ layer. Further analysis using STEM (**Fig. 8(b)**) showed the formation of twin boundaries within the diffused zirconium, and numerous dislocations in the surrounding chromium layer. Dislocation indicates the presence of significant stress within the diffused zirconium and the adjacent chromium layers, suggesting that the stress could affect the local chemical potential, and it can accelerate oxygen diffusion along the diffused zirconium.

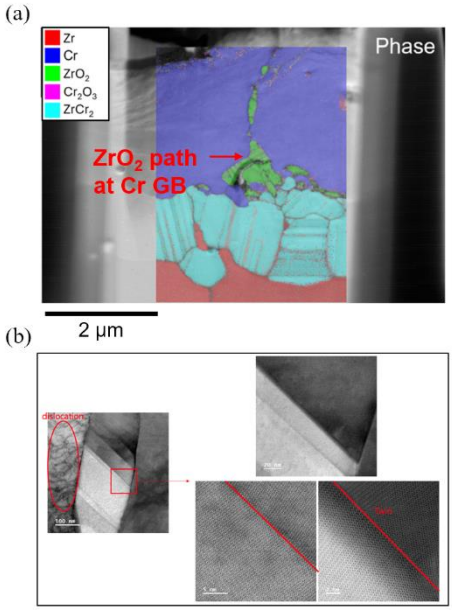

Fig. 8. TKD-TEM analysis of Cr-coated (16 μm) Zircaloy specimen oxidized at 1200 ℃ for 2.5 hours: (a) TKD phase map. (b) STEM.

3.5 Reduction of Cr_2O_3 and inner Zr oxidation

If the diffused Zr reaches the boundary of the chromium and chromium oxide layer, it transfers oxygen from the chromium oxide layer to the internal metal, partially reducing the chromium oxide layer. Since the volume of the chromium oxide layer reduces to less than half when it is reduced, numerous voids are form, creating gaps between the oxide and metal layers. It allows a significant amount of oxygen to ingress the internal zirconium. **Fig. 9** shows the EPMA mapping of zirconium of oxidized specimen with SEM image. As can be seen, a sharp zirconium signal can be found on the EPMA mapping. For the short-term oxidation (**Fig. 9(a)**), it does not reach the interface. But for the extended exposure, diffused zirconium reaches the interface, and it partially reduced the oxide layer and form many voids.

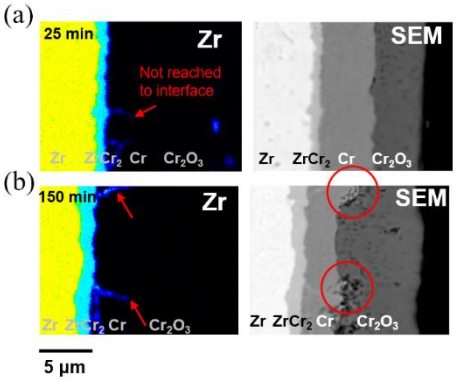

Fig. 9. EMPA mapping (Zr) and SEM image of Cr-coated (16 μm) Zircaloy during the oxidation at 1200 ℃: (a) 25 minutes. (b) 150 minutes.

The distribution of oxygen concentration of specimen oxidized at 1200 ℃ (**Fig. 10**) revealed that internal oxidation occurred. It results in an increase in oxygen concentration on the chromium-zirconium interface, and for the specimen oxidized for 150 minutes, it almost reached the saturated oxygen content of α-Zr.

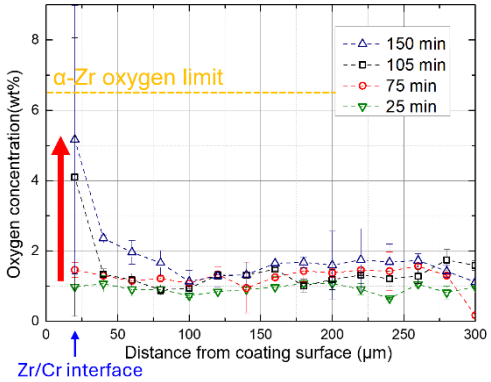

Fig. 10. Oxygen distribution of inner zirconium matrix of Cr-coated (16 μm) Zircaloy specimen oxidized at 1200 ℃.

4. Conclusion

Experiments on each key mechanism of loss of protection behavior of coating of Cr-coated ATF were conducted and the kinetic data for model development were obtained. Through the research, a framework for modeling the Cr-Zr-O diffusion system of Cr-coated ATF was derived. In addition, the newly founded characteristics of Zr path with advanced microstructure characterization with TEM and TKD were presented.

ACKNOWLEDGEMENT

This work was supported by Korea Institute of Energy Technology Evaluation and Planning (KETEP) grant funded by the Korea government (MOTIE) (No. 20224B10200100, Development of Commercialization Technology for Enhanced Accident Tolerant Fuel).

REFERENCES

[1] J.-C. Brachet, E. Rouesne, J. Ribis, T. Guilbert, S. Urvoy, G. Nony, C. Toffolon-Masclet, M. Le Saux, N. Chaabane, H. Palancher, A. David, J. Bischoff, J. Augereau, E. Pouillier, High temperature steam oxidation of chromium-coated zirconium-based alloys: Kinetics and process, Corrosion Science, Vol. 167, pp. 108537, 2020.
[2] E. Kashkarov, D. Sidelev, M. Syrtanov, C. Tang, M. Steinbrück, Oxidation kinetics of Cr-coated zirconium alloy: Effect of coating thickness and microstructure, Corrosion Science, Vol. 175, pp. 108883, 2020.
[3] H.-B. Ma, J. Yan, Y.-H. Zhao, T. Liu, Q.-S. Ren, Y.-H. Liao, J.-D. Zuo, G. Liu, M.-Y. Yao, Oxidation behavior of Cr-coated zirconium alloy cladding in high-temperature steam above 1200 °C, npj Materials Degradation Vol. 5, No. 1, pp. 7, 2021.
[4] H. Kang, D. Kim, Y. Lee, Exploring Oxidation Behavior of Chromium Coating on Zircaloy from 1100℃ to 1300℃, in preperation.
[5] D. Kim, Y. Lee, Diffusion of chromium of Cr-coated Zircaloy accident tolerant fuel cladding: Model development and experimental validation, Surface and Coatings Technology, Vol. 468, pp. 129698, 2023.